



CHORUS

This is the accepted manuscript made available via CHORUS. The article has been published as:

Ultracold Atoms in a Tunable Optical Kagome Lattice

Gyu-Boong Jo, Jennie Guzman, Claire K. Thomas, Pavan Hosur, Ashvin Vishwanath, and Dan M. Stamper-Kurn

Phys. Rev. Lett. **108**, 045305 — Published 25 January 2012

DOI: [10.1103/PhysRevLett.108.045305](https://doi.org/10.1103/PhysRevLett.108.045305)

Ultracold Atoms in a Tunable Optical Kagomé Lattice

Gyu-Boong Jo¹, Jennie Guzman¹, Claire K. Thomas¹, Pavan

Hosur¹, Ashvin Vishwanath^{1,2}, and Dan M. Stamper-Kurn^{1,2}

¹*Department of Physics, University of California, Berkeley CA 94720*

²*Materials Sciences Division, Lawrence Berkeley National Laboratory, Berkeley, CA 94720*

(Dated: November 11, 2011)

We realize a two-dimensional kagomé lattice for ultracold atoms by overlaying two commensurate triangular optical lattices generated by light at the wavelengths of 532 nm and 1064 nm. Stabilizing and tuning the relative position of the two lattices, we explore different lattice geometries including a kagomé, a one-dimensional stripe, and a decorated triangular lattice. We characterize these geometries using Kapitza-Dirac diffraction and by analyzing the Bloch-state composition of a superfluid released suddenly from the lattice. The Bloch-state analysis also allows us to determine the ground-state distribution within the superlattice unit cell. The lattices implemented in this work offer a near-ideal realization of a paradigmatic model of many-body quantum physics, which can serve as a platform for future studies of geometric frustration.

PACS numbers:

Geometrically frustrated systems with a large degeneracy of low energy states are of central interest in condensed-matter physics [1, 2]. The kagomé net – a pattern of corner-sharing triangular plaquettes – presents a particularly high degree of frustration. Such frustration impacts the kagomé quantum antiferromagnet, for which the ground state, proposed to be a quantum spin liquid or valence bond solid [3–10], remains uncertain despite decades of work. Resolving such uncertainty by experiments on solid-state kagomé magnets [11, 12] is complicated by the significant magnetic disorder or anisotropy of such materials. For this reason, more faithful realizations of quantum many-body physics in the kagomé lattice are needed.

Ultracold atoms trapped within optical lattices offer clean realizations of exotic phases of matter in condensed-matter physics [13]. Recently, non-primitive optical lattices with multiple lattice sites per unit cell have been realized in the honeycomb [14] and checkerboard [15] geometries, and double-well superlattices [16, 17], revealing non-trivial ordering and dynamics arising from a low-energy orbital degree of freedom [18]. The kagomé lattice with ultracold atoms has attracted significant interest in this context as well [19, 20], but it has not been experimentally demonstrated to our knowledge.

In this Letter, we present the realization of the kagomé geometry in a two-dimensional optical superlattice for ultracold ⁸⁷Rb atoms. The kagomé lattice is obtained by eliminating every fourth site from a triangular lattice of spacing $a/2$, with the eliminated sites forming a triangular lattice of spacing a . The remaining sites generate three connected s -orbital bands within a bandwidth on the order of the intersite tunneling energy. Intriguingly, the frustration besetting antiferromagnetic interactions also implies that one of these bands be non-dispersing. Such flat bands, distinguishing the kagomé configuration from non-primitive lattices [14–17], accentuate the role of

interparticle interactions, leading possibly to crystalline ordering [21] and supersolidity [22] for scalar bosons, and ferromagnetism of itinerant fermions [23]. Furthermore, geometric frustration of the kagomé lattice shows macroscopic degeneracy of lowest-energy classical states with XY-type antiferromagnetic interactions in contrast to the triangular lattice [24]. Our work therefore opens the door to investigations of how geometric frustration affects both orbital and magnetic properties of materials.

Our kagomé lattice is formed by overlaying short-wavelength (SW) and long-wavelength (LW) triangular lattices, formed with light at the commensurate wavelengths of 532 nm and 1064 nm, respectively [25]. In a single-wavelength lattice, formed by three plane waves of light of equal intensity I and wavevectors (and linear polarizations) lying in a plane and intersecting at equal angles, one obtains a triangular lattice of points with zero intensity, and a honeycomb lattice of points with maximum intensity $\frac{9}{2}I$ separated by a triangular lattice of intensity saddle points with intensity $4I$. Our SW lattice light is blue-detuned from the principal atomic resonances of rubidium, so that atoms are attracted to the triangular lattice of zero-intensity sites with a lattice spacing of $a/2 = (2/3) \times 532 \text{ nm} = 355 \text{ nm}$. The LW lattice is red-detuned, so that its zero-intensity points are potential-energy maxima for rubidium atoms. A unit cell of the LW lattice contains four sites of the SW triangular lattice, labeled A,B,C and D in Fig. 1. Aligning the positions of the LW potential maxima to coincide with sites D lowers the potential energies $V_{A,B,C}$ at the other sites by equal amounts $\Delta V = V_D - V_{A,B,C} = \frac{8}{9}V_{LW}$ where V_{LW} is the maximum scalar potential depth of the LW lattice (we ignore the $\sim 1\%$ vector shift in this lattice [26]). As ΔV is increased, atoms are excluded from sites D, while the remaining sites form the kagomé optical lattice. The kagomé geometry persists until $V_{LW} > 9V_{SW}$, at which point atoms become preferentially confined in

the LW honeycomb lattice.

Compared with previous proposals [19, 20], our simpler approach to creating a kagomé lattice allows one to tune the lattice geometry, thereby controlling its degree of frustration. Aligning the LW potential maxima with the SW lattice saddle points disfavors population in two sites of the four-site unit cell (e.g. $V_{B,C} < V_{A,D}$) producing a one-dimensional (1D) stripe lattice (Fig. 1c or Fig. 3a). Aligning the LW potential maxima with the SW potential maxima disfavors population in three sites of the unit cell (e.g. $V_{A,B,D} > V_C$), producing a decorated triangular lattice with lowest-energy sites forming a triangular lattice while the remaining sites form a kagomé lattice of local potential minima.

Experiments were conducted with scalar Bose-Einstein condensates of $\sim 3 \times 10^5$ ^{87}Rb atoms produced at temperatures of 80 nK in a red-detuned crossed optical dipole trap with trap frequencies of $(\omega_x, \omega_y, \omega_z) = 2\pi \times (60, 30, 350)$ Hz, with ω_z applying vertically. The large $\sim 100 \mu\text{m}$ beam-waist diameters of the lattice beams ensured that the lattice potential modified the trapping frequencies by less than 10%. Laser alignments and relative intensities were tuned to produce six-fold symmetric diffraction patterns of condensates released from LW- and SW-only lattices. The relative displacement of the LW and SW lattices was measured using two two-color Mach-Zehnder interferometers, one for beams 1 and 2 and the other for beams 1 and 3, and stabilized using piezo-actuated mirrors in the optical paths [27]. A tilted glass plate within each interferometer introduced a relative shift between the two lattice colors that, following stabilization, was imparted onto the optical lattice.

We employed atom optics to characterize the lattice as it is tuned between various geometries. These atom-optical tools presented in this work may be useful for the characterization of other superlattices and for superlattice-based atom interferometry. The first of these tools is Kapitza-Dirac diffraction [28, 29], for which the lattice potential is suddenly pulsed during τ , after which the condensate is imaged after a time of flight. The sufficiently short pulse imprints a phase $-V(\mathbf{r})\tau/\hbar$ proportional to the lattice potential $V(\mathbf{r})$ onto the condensate wavefunction (which is initially nearly uniform).

The corresponding momentum-space distribution is sensitive to the relative displacement of the LW and SW lattices. To exhibit this sensitivity we blocked one of the incident bi-chromatic lattice beams and examined the resulting one-dimensional superlattice, with potential energy given as $V(x) = V_{\text{LW}} \sin^2(qx + \delta x)/2 - V_{\text{SW}} \sin^2(qx)$ where $2\pi/q = 614 \text{ nm}$ is the 1D LW lattice spacing, and δx is the distance between the LW and SW intensity minima. The atomic populations at wavevectors $\pm q$ are given as

$$P_{\pm q} \propto \left| \pm i J_{\pm 1}^{\text{LW}} J_0^{\text{SW}} + J_{\mp 1}^{\text{LW}} J_{\pm 1}^{\text{SW}} e^{\mp i 2q\delta x} \right|^2 \quad (1)$$

where J_n is the n^{th} -order Bessel function evaluated at $\phi_{\text{LW,SW}} = V_{\text{LW,SW}} \tau / 2\hbar$, and where we consider terms up to second order in $\phi_{\text{LW,SW}}$. The lack of inversion symmetry of the lattice produced by an incommensurate value of δx appears as a left/right momentum asymmetry in the diffracted matter wave (Fig. 2).

A second method to characterize the optical superlattice is the momentum-space analysis of a superfluid occupying the ground state of the lattice potential. Here, the optical lattice potential depth was ramped up from zero over 90 ms, held constant for 100 ms, and then suddenly switched off to allow for time-of-flight expansion of the trapped gas. For the momentum-space analysis, the maximum SW potential depth was kept constant at $V_{\text{SW}}/\hbar = 40 \text{ kHz} (= 8.8 E_R)$ where E_R is the recoil energy of the SW triangular lattice. We observed no significant decay of the diffraction peak holding up to 150 ms in the optical superlattices.

Varying the relative position of the two lattices we identify the three high-symmetry lattice configurations (Fig. 3a). Given that the scalar condensate occupies the ground state of the lattice potential, its wavefunction can be taken as real and positive; thus, its momentum distribution is symmetric under inversion. Expansion from both the kagomé and the decorated triangular lattices shows the three-fold rotational symmetry of the optical superlattice. In the 1D stripe geometry, one expects equally weak occupation of two sites (e.g., A and D), and equally strong occupation of the other two sites (B and C) of the superlattice unit cell. Such a distribution is (nearly) invariant under displacements of $a/2$ along the A-D axis, and condensate diffraction along that axis should reflect the shorter periodicity of the SW lattice. The momentum distribution should also be symmetric under reflection about the A-D axis. Both traits are observed experimentally.

The Bloch-state momentum distributions allow one to quantify the ground-state wavefunction within a unit cell of the superlattice, which we express as $\psi(\mathbf{r}) = \sum_{\alpha} \psi_{\alpha} w_{\alpha}(\mathbf{r} - \mathbf{s}_{\alpha})$ where $w_{\alpha}(\mathbf{r})$ is the normalized Wannier state wavefunction, \mathbf{s}_{α} the position and $|\psi_{\alpha}|^2$ the fractional atomic population of site $\alpha \in \{A, B, C, D\}$ of the unit cell. At low $V_{\text{LW}}/V_{\text{SW}}$, we approximate $w_{\alpha} = w$ as cylindrically symmetric, Gaussian, and identical for all α . From the momentum-space populations $P_{\mathbf{G}_i}$ ($i \in \{1, 2, 3\}$) in the three first-order diffraction peaks of the LW lattice [30]—corresponding to the inner hexagon of peaks in time-of-flight images—and that at zero wavevector $P_{\mathbf{0}}$, one determines the distinct quantities

$$\tilde{P}_i = \frac{P_{\mathbf{G}_i} + P_{-\mathbf{G}_i}}{2P_{\mathbf{0}}} \frac{|\tilde{w}(\mathbf{0})|^2}{|\tilde{w}(\mathbf{G}_i)|^2} = \frac{|\psi_{\beta} + \psi_{\gamma} - \psi_{\delta} - \psi_{\epsilon}|^2}{|\sum_{\alpha} \psi_{\alpha}|^2} \quad (2)$$

where $\tilde{w}(\mathbf{0})$ and $\tilde{w}(\mathbf{G}_i)$ are now Fourier components of the Wannier function, and β, γ, δ and ϵ label the four

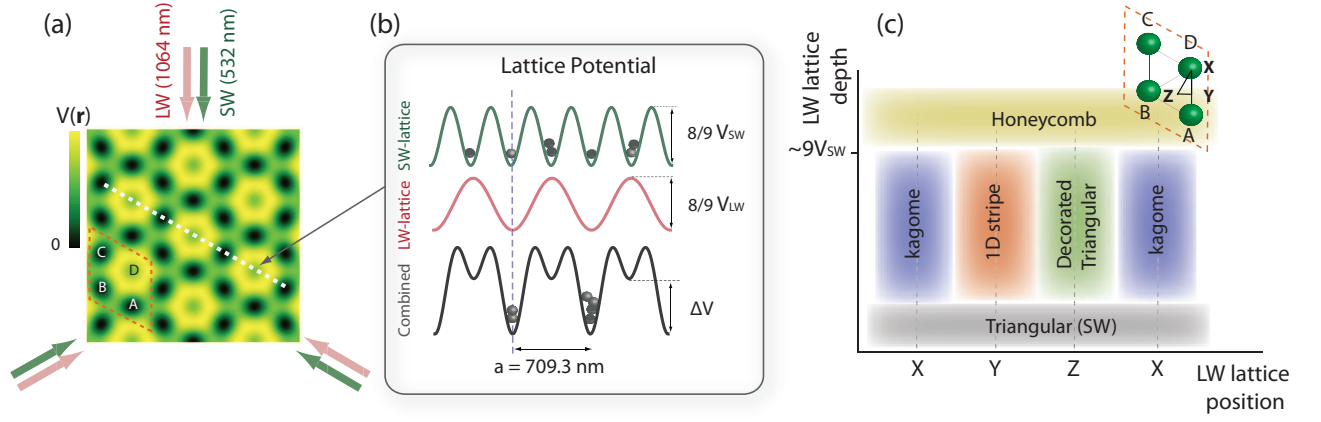


FIG. 1: Three bichromatic light beams intersecting at 120° form a kagomé optical lattice for ultracold ^{87}Rb atoms, with the two-dimensional potential $V(\mathbf{r})$ shown in (a). Profiles of the potential of the SW, LW, and combined lattices are shown in (b). Sites D of the SW lattice are emptied as ΔV exceeds the chemical potential, so that the remaining sites A, B and C form the kagomé geometry. (c) Different lattice geometries are created for intermediate LW lattice depths ($V_{LW} < 9V_{SW}$) by displacing the potential maxima of the SW lattice to the high-symmetry points X, Y or Z within the unit cell. For higher LW lattice depths, a honeycomb geometry prevails.

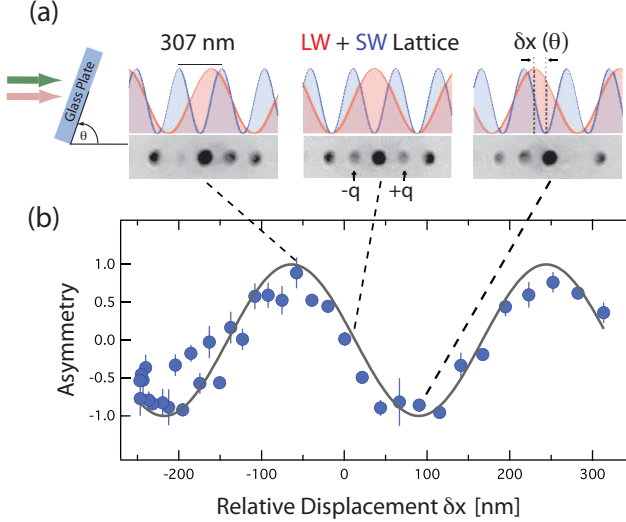


FIG. 2: Atom diffraction patterns, formed by $\tau = 8 \mu\text{s}$ pulse of the lattice potential (with $V_{SW}/h \sim 80\text{kHz}$ and $V_{LW}/h \sim 50\text{kHz}$) followed by 26 ms time of flight, exhibit left/right momentum asymmetry (defined as $(P_{+q} - P_{-q}) / (P_{+q} + P_{-q})$) that varies with the displacement δx between the LW- and SW-lattice intensity minima, in close agreement with the predicted behavior (solid line).

sites so that $\mathbf{G}_i \cdot (\mathbf{s}_\beta - \mathbf{s}_\gamma) = 0$. The Wannier state Fourier components in Eq. 2 are determined from the second-order diffraction populations as $|\tilde{w}(\mathbf{0})|^2 / |\tilde{w}(\mathbf{G}_i)|^2 = (2P_0 / (P_{2\mathbf{G}_i} + P_{-2\mathbf{G}_i}))^{1/4}$. Together with the normalization $\sum_\alpha |\psi_\alpha|^2 = 1$ these quantities determine the atomic distribution in the unit cell [31].

We measured the population ratios \tilde{P}_i as the superlattice geometry was gradually tuned. Translating the rel-

ative position of the two lattices (Fig. 3b), one advances from the kagomé geometry, with equal population in the three ratios, to the 1D stripe geometry, with two identically small ratios, and then to another kagomé-geometry lattice. Our data agree with a calculation of the single-particle ground-state for the known lattice depths.

We focus finally on the kagomé-geometry lattice alignment, and examine the transition between the triangular and kagomé geometries (Fig. 4). At zero V_{LW} , the atoms are confined in a SW triangular lattice, and the first-order LW lattice diffraction orders are absent, indicating a unit-cell population of $(A, B, C, D) = (1/4, 1/4, 1/4, 1/4)$. As the LW lattice depth is increased, the population ratios \tilde{P}_i increase and the kagomé geometry is achieved by gradually expelling atoms from one site of the unit cell. The population ratios tend toward a limiting value of $1/9$ that is a hallmark of diffraction from a kagomé lattice wherein the atoms are distributed as $(A, B, C, D) = (1/3, 1/3, 1/3, 0)$.

Here, the ground state of the kagomé lattice does not suffer from frustration. In the future, effects of frustration may be explored by transferring bosons into the excited s -orbital flat band, or by changing the sign of the hopping energy [32] so that the flat band becomes the lowest in energy. The present choice of wavelengths also yields kagomé lattices for the fermionic isotopes ^6Li and ^{40}K . Introducing fermions into the lattice at the appropriate fillings would place the Fermi energy within the flat band, allowing for studies of flat-band ferromagnetism due to repulsive interactions [23] or enhanced Cooper pairing for attractive interactions [33]. Also, the demonstrated tunability of the superlattice opens new possibilities to emulate both ideal and deliberately distorted kagomé lattices, potentially stabilizing the various candidate ground states of the kagomé quantum antiferro-

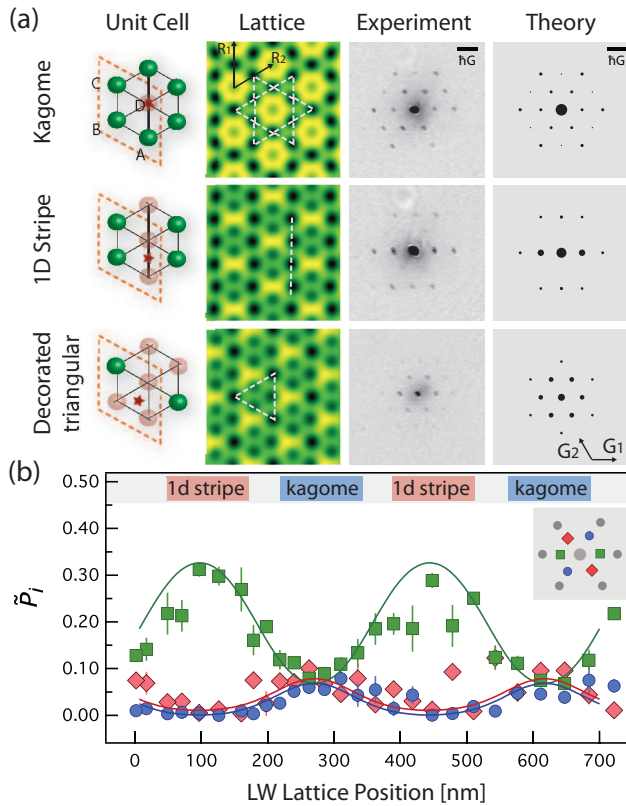


FIG. 3: The real- and momentum-space composition of a superfluid for various lattices. (a) The kagomé and decorated triangular lattices maintain three-fold rotational symmetry in configuration and momentum space, while the symmetry of the 1D stripe lattice is reduced to a parity symmetry (left-right in the images). For each setting, a schematic distinguishes between sites of high (green) and low (red) atomic population. The expected momentum distribution for measured values of $V_{\text{SW}}/h = 40\text{kHz}$ and $\Delta V/h = 14\text{kHz}$ is shown with the area of the black dot reflecting the fractional population. (b) Translating the LW-lattice potential maxima (marked as a star in the schematic) along the A-D axis tunes the lattice between kagomé and 1D stripe geometries, as revealed by the population ratios \tilde{P}_i identified according to the inset. The data (averages of 4-5 measurements) agree with calculations of the single-particle ground state (solid lines) with the lattice depth used in the experiment. Interaction effects are neglected since ΔV was higher than the chemical potential $\mu \sim h \times 3.5\text{kHz}$ of the condensate in the SW-only lattice.

magnet.

We thank S. Schreppler for experimental assistance. C. K. Thomas acknowledges support by the Department of Energy Office of Science Graduate Fellowship Program (DOE SCGF), made possible in part by the American Recovery and Reinvestment Act of 2009, administered by ORISE-ORAU under contract DE-AC05-06OR2310. P. H. was supported by NSF-DMR 0645691. This work was supported by the NSF and by the Army Research Office with funding from the DARPA OLE program.

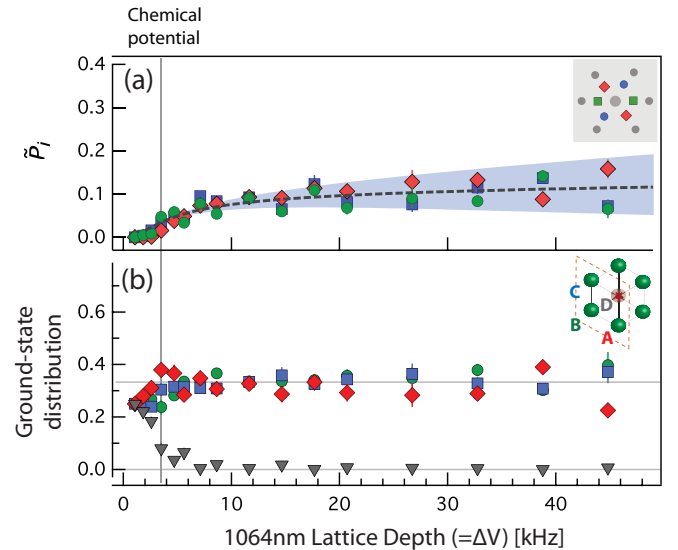


FIG. 4: The superlattice was converted from a SW triangular to a kagomé lattice by increasing V_{LW} . As ΔV exceeds the condensate chemical potential ($\mu/h \simeq 3.5\text{kHz}$), (a) the momentum population ratios reach the asymptotic value of $1/9$ expected for a kagomé lattice, and (b) the D-site population is extinguished. Data points represent averages of 7-10 measurements. In (a), the dashed curve indicates the predicted \tilde{P}_i while the shaded region indicates the expected variation in \tilde{P}_i given a shot-to-shot instability of $\sim 20\text{nm}$ in the relative position of the LW and SW lattices.

-
- [1] A. P. Ramirez, *Annu Rev Mater Sci* **24**, 453 (1994).
- [2] L. Balents, *Nature* **464**, 199 (2010).
- [3] V. Elser, *Phys. Rev. Lett.* **62**, 2405 (1989).
- [4] J. B. Marston and C. Zeng, *J. Appl. Phys.* **69**, 5962 (1991).
- [5] S. Sachdev, *Phys. Rev. B* **45**, 12377 (1992).
- [6] P. Nikolic and T. Senthil, *Phys. Rev. B* **68**, 214415 (2003).
- [7] F. Wang and A. Vishwanath, *Phys. Rev. B* **74**, 174423 (2006).
- [8] Y. Ran et al., *Phys. Rev. Lett.* **98**, 117205 (2007).
- [9] R. R. P. Singh and D. A. Huse, *Phys. Rev. B* **76**, 180407 (2007).
- [10] S. Yan, D. A. Huse, and S. R. White, *Science* **332**, 1173 (2011).
- [11] M. P. Shores et al., *J Am Chem Soc* **127**, 13462 (2005).
- [12] Z. Hiroi et al., *J. Phys. Soc. Jpn.* **70**, 3377 (2001).
- [13] I. Bloch, J. Dalibard, and W. Zwerger, *Reviews of Modern Physics* **80**, 885 (2008).
- [14] P. Soltan-Panahi et al., *Nat Phys* **7**, 434 (2011).
- [15] G. Wirth, M. Olschlager, and A. Hemmerich, *Nat Phys* **7**, 147 (2011).
- [16] J. Sebby-Strabley et al., *Phys. Rev. A* **73**, 033605 (2006).
- [17] S. Folling et al., *Nature* **448**, 1029 (2007).
- [18] P. Soltan-Panahi, D.-S. Luhmann, J. Struck, P. Windpassinger, and K. Sengstock, *Nat Phys* (2011), 10.1038/nphys2128.
- [19] L. Santos et al., *Phys. Rev. Lett.* **93**, 030601 (2004).
- [20] J. Ruostekoski, *Phys. Rev. Lett.* **103**, 080406 (2009).
- [21] C. J. Wu et al., *Phys. Rev. Lett.* **99**, 070401 (2007).
- [22] S. D. Huber and E. Altman, *Phys. Rev. B* **82**, 184502 (2010).
- [23] H. Tasaki, *Phys. Rev. Lett.* **69**, 1608 (1992).
- [24] J. Struck, C. Ischlger, R. Le Targat, P. Soltan-Panahi, A. Eckardt, M. Lewenstein, P. Windpassinger, and K. Sengstock, *Science* **333**, 996 (2011).
- [25] While the SW and LW wavelengths of 532.15 nm and 1063.96 nm are not perfectly commensurate, the relative displacement of the SW and LW lattices varies by only (18,9) nm over the $(d_x, d_y) = (28, 14) \mu\text{m}$ transverse diameter of the condensate.
- [26] J. Dalibard and C. Cohen-Tannoudji, *J. Opt. Sci. Am. B* **6**, 2023 (1989).
- [27] For Kaptiza-Dirac diffraction, stabilization was engaged with the lattice at negligible intensity before the brief high-intensity pulse. For Bloch-state analysis, stabilization was engaged upon the ramp-on of the lattice beams.
- [28] P. Gould, G. Ruff, and D. Pritchard, *Phys. Rev. Lett.* **56**, 827 (1986).
- [29] Y. B. Ovchinnikov et al., *Phys. Rev. Lett.* **83**, 284 (1999).
- [30] Momentum populations of condensed atoms are measured by integrating under the narrow time-of-flight atomic distributions. The contribution from the thermal atoms is subtracted, thereby accounting for finite-size, finite-temperature, and interaction effects during the expansion of the gas.
- [31] We assume that all atoms lie in the ground band of the lattice potential with constant phase. Inverting Eqs. 2 gives a discrete degeneracy of solutions that is resolved by knowledge of the approximate populations.
- [32] H. Lignier et al., *Phys. Rev. Lett.* **99**, 220403 (2007).
- [33] M. Imada and M. Kohno, *Phys. Rev. Lett.* **84**, 143 (2000).